

---

# HIGH-PERFORMANCE PARTIAL SPECTRUM COMPUTATION FOR SYMMETRIC EIGENVALUE PROBLEMS AND THE SVD

---

A PREPRINT

David Keyes\*

Hatem Ltaief\*

Yuji Nakatsukasa<sup>†</sup>Dalal Sukkari<sup>‡</sup>

November 25, 2021

**ABSTRACT**

Current dense symmetric eigenvalue (EIG) and singular value decomposition (SVD) implementations may suffer from the lack of concurrency during the reduction step toward the corresponding condensed matrix forms, i.e., tridiagonal and bidiagonal, respectively. This performance bottleneck is typical for the two-sided transformations due to the Level-2 BLAS calls. These memory-bound functions are inherently limited by the speed of the bus bandwidth and may already saturate the memory bandwidth with only a small number of processes. Therefore, the current state-of-the-art EIG and SVD implementations may achieve only a small fraction of the system's sustained peak performance. The QR-based Dynamically Weighted Halley (QDWH) algorithm may be used as a pre-processing step toward the EIG and SVD solvers, while mitigating the aforementioned bottleneck. QDWH-EIG and QDWH-SVD expose more parallelism, while relying on compute-bound matrix operations. Both run closer to the sustained peak performance of the system, but at the expense of performing more floating-point operations than the standard EIG and SVD algorithms. These algorithms are designed to compute the full SVD and eigendecomposition. In this paper, we introduce a new QDWH-based solver for computing the partial spectrum for EIG (QDWH<sub>partial</sub>-EIG) and SVD (QDWH<sub>partial</sub>-SVD) problems. By optimizing the rational function underlying the algorithms only in the desired part of the spectrum, QDWH<sub>partial</sub>-EIG and QDWH<sub>partial</sub>-SVD algorithms efficiently compute a fraction (say 1–20%) of the eigenspectrum as well as the most significant singular values/vectors, respectively. We develop high-performance implementations of QDWH<sub>partial</sub>-EIG and QDWH<sub>partial</sub>-SVD on distributed-memory manycore systems and demonstrate their numerical robustness. We perform a benchmarking campaign against their counterparts from the state-of-the-art numerical libraries (i.e., ScaLAPACK, ELPA, KSVD) across various matrix sizes using up to 36K MPI processes. Experimental results show performance speedups for QDWH<sub>partial</sub>-SVD up to 6X and 2X against PDGESVD from ScaLAPACK and KSVD, respectively. QDWH<sub>partial</sub>-EIG outperforms PDSYEV from ScaLAPACK up to 3.5X but remains slower compared to ELPA. QDWH<sub>partial</sub>-EIG achieves, however, a better occupancy of the underlying hardware by extracting higher sustained peak performance than ELPA, which is critical moving forward with accelerator-based supercomputers.

**Keywords** QDWH · Symmetric Eigensolver · Singular Value Decomposition · Partial Spectrum Calculation · High Performance Computing

**1 Introduction**

Solving the dense symmetric eigenvalue (EIG) and singular value decomposition (SVD) problems [1, 2, 3] represent one of the main computational phases for many scientific problems, e.g., signal processing [4], pattern recognition [5],

---

\*King Abdullah University of Science and Technology, Extreme Computing Research Center, Computer, Electrical, and Mathematical Sciences and Engineering Division, Thuwal, 23955-6900, Saudi Arabia (David.Keyes, Hatem.Ltaief@kaust.edu.sa).

<sup>†</sup>Mathematical Institute, University of Oxford, Oxford OX2 6GG, UK (Yuji.Nakatsukasa@maths.ox.ac.uk).

<sup>‡</sup>Innovative Computing Laboratory, University of Tennessee, Knoxville TN 37996, USA (sukkari@icl.utk.edu).

statistics [6], quantum chemistry [7], quantum physics [8], and quantum mechanics [9]. There are actually many applications for which there is interest in extracting only a partial eigenspectrum from EIG, e.g., in density function theory for electronic structure calculations [10]. Similarly, there are several numerical algorithms that may only require the most significant singular values with their associated singular vectors from SVD, e.g., determining the pseudo-inverse of a matrix [11] or performing low-rank matrix approximations [12, 13, 14].

The current state-of-the-art numerical libraries LAPACK [15] and ScaLAPACK [16] for shared-memory and distributed-memory systems, respectively, provide EIG and SVD implementations. They first reduce the original dense matrix into condensed tridiagonal and bidiagonal forms, before computing the eigenspectrum and the singular values/vectors, respectively. Although this initial reduction phase occupies a small part of the floating-point operations (flops), it may still account for up to half of the overall time taken by the EIG and SVD solvers. This is due to its memory-bound execution during the expensive panel factorization based on Level-2 BLAS, which requires accessing the entire unreduced trailing submatrix. The memory bandwidth may quickly become saturated and adding more computational resources may actually slow down further the execution. Two-stage matrix reductions [17, 18] for EIG and SVD have become popular, as they allow to cast some of the Level-2 BLAS operations into compute-bound Level-3 BLAS.

In many applications, one is interested only in a subset of the spectrum; usually the extremal (largest/smallest) eigenpairs and the dominant singular triplets. However, the traditional one/two-stage reduction-based approaches still require to transform the whole matrix into tridiagonal or bidiagonal form, so the overall runtime is comparable to that of a full decomposition.

In this paper, we design and implement algorithms that remove these aforementioned limitations in order to compute the partial spectrum for the EIG and SVD solvers. Based on the polar decomposition, these new high performance EIG and SVD algorithms rely on the QR-based Dynamically Weighted Halley (QDWH) method to compute a partial spectrum. As initially introduced in [19], QDWH is an expensive approach with a much higher number of flops when used toward computing the full spectrum for EIG and SVD solvers [20]. But ultimately, it turns out to be a competitive approach for SVD, while remaining an interesting alternative for EIG [21, 22, 23]. The main idea consists in compensating for these extra flops with the higher level of concurrency and the compute-bound nature achieved by the QDWH numerical kernels. We then leverage existing QDWH-based SVD and EIG algorithms to compute the partial spectrum for the EIG (QDWH<sub>partial</sub>-EIG) and SVD (QDWH<sub>partial</sub>-SVD). Our new QDWH<sub>partial</sub>-EIG and QDWH<sub>partial</sub>-SVD algorithms permit to redirect the computational power toward only the operations necessary for the computation of the spectrum of interest. This inherent flexibility of QDWH makes it even more competitive against the existing implementations for extracting the partial spectrum for the EIG.

We deploy both QDWH<sub>partial</sub>-EIG and QDWH<sub>partial</sub>-SVD implementations on a large distributed-memory system and ensure the original numerical robustness of QDWH-based full EIG and SVD is maintained, for various matrix types. We then assess their individual performance and compare them against their respective counterparts from the state-of-the-art numerical libraries (i.e., ScaLAPACK [16], ELPA [24], and KSVD [23]). Experimental results show performance speedups for QDWH<sub>partial</sub>-SVD up to 6X and 2X against PDGESVD from ScaLAPACK and KSVD, respectively. QDWH<sub>partial</sub>-EIG outperforms PDSYEV from ScaLAPACK up to 2.5X while being within reach compared to ELPA. Moreover, QDWH<sub>partial</sub>-EIG is capable to extract a higher sustained peak performance from the underlying hardware. This is critical when looking at hardware architecture trends, where accelerator-based systems generously provisioned with flops will constitute most of recently announced exascale supercomputers.

The remainder of the paper is organized as follows. Section 2 describes related work for state-of-the-art EIG and SVD solvers. Section 3 reviews the background of the QDWH approach for the polar decomposition and its application to EIG and SVD solvers. Section 4 introduces the new QDWH<sub>partial</sub>-EIG and QDWH<sub>partial</sub>-SVD algorithms for computing only the partial spectrum. Section 5 describes the implementation details and Section 6 estimates the algorithmic operation counts. Section 7 highlights the numerical robustness of both QDWH<sub>partial</sub>-EIG and QDWH<sub>partial</sub>-SVD algorithms. Section 8 assesses the achieved performance results and we conclude in Section 9.

## 2 Related work

When computing the *full* spectrum for symmetric (or Hermitian for complex matrices) eigenvalue and SVD solvers, the state-of-the-art approaches can be split into two categories. The one-stage approaches, as implemented in LAPACK [15] and ScaLAPACK [16], reduce the dense matrix into a condensed form using a single phase of orthogonal transformations, before extracting the spectrum of interest. To further promote Level-3 BLAS operations during this single stage, two-stage approaches [17, 18] have emerged as an efficient algorithmic alternative in better extracting the hardware performance. Although they come at the price of extra floating-point operations (flops), their high performance implementations have contributed in their wide adaption in the software ecosystem within the PLASMA [25, 26, 27, 28, 29, 30]

and MAGMA [31] libraries on shared-memory systems (possibly equipped with GPUs) for eigenvalue and SVD solvers or the ELPA [24] and EigenExa [32] libraries for only eigenvalue solvers on distributed-memory systems.

When it comes to calculating the *partial* spectrum for eigenvalue and SVD solvers, the one and two-stage approaches are inefficient as described above. A more recent work [33] shows how to partially compute the SVD out of the bidiagonal form using an associated tridiagonal eigenproblem. But yet again, the condensed form remains the ultimate starting point and one of the most expensive computational operations.

Completely different classes of algorithms for computing a small part of the spectrum have been developed, most prominently the Lanczos algorithm (more generally Krylov subspace methods) and the more recent randomized algorithms [34]. While these can be very powerful, they come with certain drawbacks in the situation that we consider.

Krylov methods are usually suitable only when a very small fraction of the spectrum (usually  $O(1)$  eigenvalues or singular values) is required, and sometimes fails to provide full accuracy. In this work we consider the case where a nonnegligible portion of the spectrum (say 1 – 20%) is desired.

Randomized algorithms can be an extremely effective means of finding an approximate SVD, and are rapidly gaining popularity. However, they usually come with poorer accuracy guarantees, giving outputs that are suboptimal by an  $O(1)$  factor; see [34, §10], [35, §3] (these guarantees are still remarkable—especially when the spectrum decays rapidly—and enough in many applications [12]).

In this paper, we propose to revisit and modify the QDWH-EIG/SVD algorithms [19, 20] in order to provide support for determining only a partial spectrum for the eigenvalue and SVD solvers. We aim to compute the eigen/singular values and vectors essentially to full working precision. These algorithms and their high performance implementations [22, 21, 23, 36] do not require a reduction to tridiagonal or bidiagonal forms. They iteratively compute the polar decomposition—based on conventional, compute-bound, and highly-parallel dense linear algebra operations—as a preprocessing step toward the eigenvalue and SVD solvers. By altering the core algorithmic feature of QDWH-EIG/SVD, the new QDWHpartial-EIG/SVD approach transforms directly the original dense matrix to a much smaller one, with a size roughly of the spectrum of interest. Since the transformation occurs at the beginning of the QDWHpartial-EIG/SVD procedure, the power of computational resources is tailored solely to operations that are intimately related to the eigenspace of interest.

### 3 QDWH-based polar decomposition and its application to full symmetric eigenvalue and SVD solvers

The Polar Decomposition (PD)  $A = U_p H \in \mathbb{C}^{m \times n}$ , where  $U_p \in \mathbb{C}^{m \times n}$  is the *unitary polar factor* with  $U_p^* U_p = I_n$  and  $H$  is Hermitian positive semidefinite, exists for any matrix. It is an important matrix decomposition for various applications, including inertial navigation [37], chemistry [38], and computation of block reflectors in numerical linear algebra [39]. It can be used as a first computational phase toward computing the EIG/SVD [20] in the context of the QR-based Dynamically Weighted Halley (QDWH) method.

#### 3.1 The QDWH-Based PD Algorithm

The dynamically weighted Halley iteration to find the PD can be summarized as follows:

$$\begin{aligned} X_0 &= A/\alpha, \\ X_{k+1} &= X_k(a_k I + b_k X_k^* X_k)(I + c_k X_k^* X_k)^{-1}. \end{aligned} \tag{1}$$

The scalars  $(a_k, b_k, c_k)$  are chosen dynamically to speed up the convergence [19]. More specifically, they are chosen so that the rational function  $r_k(x) = x(a_k + b_k x^2)/(1 + c_k x^2)$  is the scaled *Zolotarev* function of type  $(3, 2)$ , the best rational approximation to the sign function on  $[-1, -\ell_k] \cup [\ell_k, 1]$ . Here  $\ell_0 = 1/\kappa_2(A)$  (or its estimate) and follows the updating formula  $\ell_k = r_k(\ell_{k-1})$ . The singular values of  $X_k$  are  $\Sigma_k = r_k(\cdots r_2(r_1(\Sigma)))$ , and lie in  $[\ell_k, 1]$ . Remarkably, the composition of the rational functions  $r_k(\cdots r_2(r_1(\Sigma)))$  is again a Zolotarev function, of much higher type  $(3^k, 3^k - 1)$ . Together with the exponential convergence of Zolotarev functions, QDWH converges in at most *six* iterations to obtain  $X_k \rightarrow U_p$  (and  $\ell_k \rightarrow 1$ ) in double precision for matrices with  $\kappa_2(A) \leq 10^{15}$ .

Based on the fact [40, p. 219] that  $cX(I + c^2 X^* X)^{-1} = Q_1 Q_2^*$ , where  $\begin{bmatrix} cX \\ I \end{bmatrix} = \begin{bmatrix} Q_1 \\ Q_2 \end{bmatrix} R$  is the *QR* decomposition, with  $X, Q \in \mathbb{R}^{m \times n}$  and  $Q_2, R \in \mathbb{R}^{n \times n}$ , the Equation (1) can be replaced with the following inverse-free and stable

QR-based implementation [20]:

$$\begin{aligned} \begin{bmatrix} \sqrt{c_k} X_k \\ I \end{bmatrix} &= \begin{bmatrix} Q_1 \\ Q_2 \end{bmatrix} R, \\ X_{k+1} &= \frac{b_k}{c_k} X_k + \frac{1}{\sqrt{c_k}} \left( a_k - \frac{b_k}{c_k} \right) Q_1 Q_2^*. \end{aligned} \quad (2)$$

This represents the QR-based Dynamically Weighted Halley (QDWH) algorithm. Further details can be found in [41]. After a few QDWH iterations from Equation (2), the  $X_k$  eventually becomes well-conditioned and  $\ell_k = O(1)$ . Once this happens, a lower-cost Cholesky-based iteration can be used instead, as follows:

$$\begin{aligned} X_{k+1} &= \frac{b_k}{c_k} X_k + \left( a_k - \frac{b_k}{c_k} \right) (X_k W_k^{-1}) W_k^{-*}, \\ W_k &= \text{chol}(Z_k), \quad Z_k = I + c_k X_k^* X_k. \end{aligned} \quad (3)$$

A higher-order variant of the QDWH algorithm that employ higher-degree Zolotarev functions has been developed [41], which further increases the degree of parallelism.

### 3.2 Applying QDWH to Full Symmetric Eigenvalue and SVD Solvers

First, we recall the mechanism of QDWH-EIG [20], on which the new QDWHpartial-EIG algorithm will be based. Let  $A$  be an  $n \times n$  symmetric matrix and write

$$\begin{aligned} A &= V \text{diag}(\Lambda_+, \Lambda_-) V^* \\ &= V \text{diag}(I_{n-k}, -I_k) V^* \cdot V \text{diag}(\Lambda_+, |\Lambda_-|) V^* \\ &\equiv U_p H, \end{aligned} \quad (4)$$

where  $U_p H$  is the polar decomposition [40, Ch. 8].  $k$  is the number of negative eigenvalues, which we do not assume to be known. Suppose that the unitary polar factor  $U_p$  is computed. This means we have mapped all the eigenvalues to 1 or  $-1$ . We partition  $V = [V_+, V_-]$  conformably with  $\Lambda$ , and note that

$$\begin{aligned} \frac{1}{2}(I - U_p) &= \frac{1}{2} \left( I - [V_+ \ V_-] \begin{bmatrix} I_{n-k} & 0 \\ 0 & -I_k \end{bmatrix} [V_+ \ V_-]^* \right) \\ &= [V_+ \ V_-] \begin{bmatrix} 0 & 0 \\ 0 & I_k \end{bmatrix} [V_+ \ V_-]^* \\ &= V_- V_-^*. \end{aligned} \quad (5)$$

Hence the symmetric matrix  $C = \frac{1}{2}(I - U_p) = V_- V_-^*$  is an orthogonal projector onto  $\text{Span}(V_-)$ , the invariant subspace corresponding to the negative eigenvalues. We can then project the matrix  $A$  (Rayleigh-Ritz process) to obtain the eigenvalues and eigenvectors: the eigenvalues of  $V_-^* A V_-$  are equal to those of  $\Lambda_-$ , and denoting by  $V_-^* A V_- = W \Lambda_- W^*$  the eigenvalue decomposition, we see that  $V_- W$  is the matrix of eigenvectors. Analogously, we can obtain  $V_+$  by finding the subspace spanned by  $\frac{1}{2}(I + U_p)$ .

Second, the polar decomposition can be also used directly toward calculating the SVD, i.e.,  $A = U_p H = U_p (V \Sigma V^*) = (U_p V) \Sigma V^T = U \Sigma V^*$  where  $\Sigma$  is the matrix containing all the singular values, and  $U$  and  $V$  are the orthogonal matrices containing the left and right singular vectors, respectively. The resulting QDWH-SVD procedure relies on QDWH-EIG (or any other eigensolvers) to compute the intermediate eigendecomposition  $H = V \Sigma V^*$  required for the final SVD.

## 4 Leveraging QDWH for computing the partial spectrum of symmetric eigenvalue and SVD solvers

In this section, we present modified versions of QDWH-EIG and QDWH-SVD to compute the partial (negative) eigen-spectrum of a symmetric matrix (QDWHpartial-EIG) and to extract the most significant singular values and their corresponding singular vectors (QDWHpartial-SVD).

In what follows we treat nonreal matrices  $A \in \mathbb{C}^{n \times n}$ ; when  $A$  is real, the superscripts  $\cdot^*$  should be replaced by  $\cdot^T$  and everything can be executed using only real arithmetic.

#### 4.1 QDWHpartial-EIG

We introduce QDWHpartial-EIG, an algorithm for computing the negative eigenvalues and its corresponding eigenvectors (of course the algorithm can be modified trivially to find the eigenvalues/vectors smaller/larger than any specific number by shifting and scaling by  $-1$ ).

For simplicity of exposition, here we suppose that the negative eigenvalues lie (roughly) in  $[-1, 0)$ , that is,  $\lambda_{\min}(A) \gtrsim -1$ . To ensure this we need a lower bound  $\mu \leq \lambda_{\min}(A) < 0$ ; many algorithms are available for this task; we use a few steps of the Lanczos iteration to estimate  $\lambda_{\min}(A)$ . We then scale the matrix  $A := A/|\mu|$ .

Recall that the mathematics underlying the QDWH-EIG algorithm is rational approximation: it finds a rational function  $r$  that approximates the sign function, so that it maps the negative eigenvalues to  $-1$ , and positive eigenvalues to  $1$ . Thus  $r(A)$  has eigenvalues  $\pm 1$ .

Now, suppose that we only need the negative eigenspace  $V_-$ . Can we cut corners? The answer is yes—and this is not just that we can skip computing  $V_*$  once  $U_p$  is computed. We shall avoid computing  $U_p$ . Essentially, we need to ensure only that the negative eigenvalues have been mapped to  $-1$ ; the positive eigenvalues are irrelevant. Namely, the idea is to find a matrix whose null space  $Q_2$  contains  $V_-$ . We then extract  $V_-$  as a subspace of  $Q_2$ .

To obtain such  $Q_2$  efficiently, a key idea is to only map the required eigenvalues by the sign function. QDWH works on the interval  $[-1, -\ell_0] \cup [\ell_0, 1]$  and approximates the sign function there with a rational function  $r$ ; the QDWH convergence is governed by  $\ell_0$ ; the larger the faster.

Now, we can use the *shifted* rational function  $r(x - s)$  for some  $s \in (0, 1)$ ; if  $r$  approximates the sign function on  $[-1, -s] \cup [s, 1]$  (taking  $\ell_0 = s$ ), then we have  $r(x - s) \approx -1$  on  $[-1 + s, 0]$ . Therefore, defining  $\tilde{A} := (1 - s)A - sI$  (whose negative eigenvalues are again in  $[-1, 0]$ , and the negative eigenvalues of  $A$  correspond to those of  $\tilde{A}$  in  $[-1, -s]$ ), we see that the negative eigenvalues of  $A$  are mapped to  $-1$  by  $r(\tilde{A})$ .

The reason we introduce the shift  $s$  is that we can then set  $\ell_0 = s$ , so QDWH can converge faster with a low-degree Zolotarev function. For illustration, Fig. 1 shows a typical plot of  $r(x - s)$ . Observe how the interval  $[-1, 0]$  is mapped to  $-1$  with a low-degree rational function.

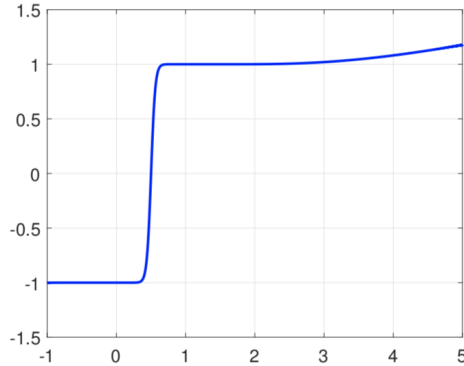


Figure 1: A type (9, 8) rational function  $y = r(x - s)$  that maps the interval  $[-1, 0]$  to  $-1$ .  $s = 0.5$ .

Suppose that we have computed the matrix function  $r(\tilde{A})$ . It has  $k$  (or more) eigenvalues at  $-1$ , where  $k$  is the number of negative eigenvalues of  $A$ . Since the desired eigenvalues have been mapped to  $-1$ , we are interested in the null space of  $r(\tilde{A}) + I$ . While  $r(\tilde{A})$  has  $n - k$  (or fewer) eigenvalues away from  $-1$ , the knowledge of their precise values is not critical. It does matter, however, that they do not blow up to  $\pm\infty$ , for numerical stability.

It is worth emphasizing that there is a nontrivial interval on the positive side (on  $[0, \hat{s}]$  for  $\hat{s} < s$ ) that is mapped close to  $-1$ . This is an inevitable nature of rational functions, and can cause the dimension of the numerical null space of the matrix  $r(\tilde{A}) + I$  to be larger than  $k$ . Indeed if we take  $s$  too large to a point where all the eigenvalues of  $A$  are mapped close to  $-1$ , then  $r(\tilde{A}) + I$  converges to zero, and the process below leads to no efficiency gain (i.e., the whole space becomes the computed null space and no gain is obtained relative to doing a full eigendecomposition). We discuss how to choose an appropriate  $s$  shortly.

We then work with the matrix  $r(\tilde{A}) + I$ . This matrix is not a partial isometry as it was in QDWH, but it is still rank deficient, with deficiency  $k$  or more.

To compute the null space of  $r(\tilde{A}) + I$  (or a larger subspace that contains it), we compute the QR factorization

$$r(\tilde{A}) + I = [Q_1, Q_2] \begin{bmatrix} R_{11} & R_{12} \\ 0 & R_{22} \end{bmatrix} \quad (6)$$

where the size of  $R_{11}$  (and hence of  $R_{22} \in \mathbb{C}^{\ell \times \ell}$ , where  $\ell \geq k$ ) is chosen so that it only has “large” singular values; the idea is that  $Q_2$  then contains the null space of  $A$  that we require. To quantify the claim we use matrix perturbation theory.

**Theorem 1** *Let  $B = [Q_1, Q_2] \begin{bmatrix} R_{11} & R_{12} \\ 0 & R_{22} \end{bmatrix} \in \mathbb{C}^{m \times n}$  ( $m \leq n$ ) be a full QR factorization such that  $[Q_1, Q_2] \in \mathbb{C}^{m \times m}$  is unitary with  $Q_2 \in \mathbb{C}^{m \times \ell}$  and  $R_{11} \in \mathbb{C}^{(m-\ell) \times (m-\ell)}$ . Let  $V_0 \in \mathbb{C}^{m \times k}$  have orthonormal columns  $V_0^* V_0 = I_k$ , with  $k \leq \ell$ . Then*

$$\sin \angle(V_0, Q_2) \leq \frac{\|V_0^* B\|_2}{\sigma_{\min}(R_{11})}. \quad (7)$$

*Remark.* The main situation of interest is when  $V_0$  spans an approximate left null space of  $B$  such that  $\|V_0^* B\|_2 = O(u\|B\|_2)$ , where  $u$  is unit roundoff; then the theorem shows the subspace  $V_0$  is approximately contained in  $Q_2$ , up to  $O(u/\sigma_{\min}(R_{11}))$ .

PROOF. First recall that the canonical angles  $\angle_1(V_0, Q_1), \dots, \angle_k(V_0, Q_1)$  between two subspaces of dimensions  $k, \ell$  ( $\ell \geq k$ ) spanned by the orthonormal matrices  $V_0 \in \mathbb{C}^{m \times k}$  and  $Q_2 \in \mathbb{C}^{m \times \ell}$  (for which  $Q_1$  is the orthogonal complement  $Q_1^* Q_2 = 0$ ) are defined by  $\sin \angle_i(V_0, Q_1) = \sigma_i(V_0^* Q_1)$  [2, § 2] for  $i = 1, \dots, k$ . It thus suffices to show that  $\|V_0^* Q_1\|_2 \leq \frac{\|V_0^* B\|_2}{\sigma_{\min}(R_{11})}$ .

Now we have

$$V_0^* B = [V_0^* Q_1, V_0^* Q_2] \begin{bmatrix} R_{11} & R_{12} \\ 0 & R_{22} \end{bmatrix} = [V_0^* Q_1 R_{11}, V_0^* Q_1 R_{12} + V_0^* Q_2 R_{22}].$$

Hence we obtain  $\|V_0^* B\|_2 \geq \|V_0^* Q_1 R_{11}\|_2 \geq \|V_0^* Q_1\|_2 \sigma_{\min}(R_{11})$ . It follows that  $\|V_0^* Q_1\|_2 \leq \frac{\|V_0^* B\|_2}{\sigma_{\min}(R_{11})}$ , as required.  $\square$

Let us make two remarks about the theorem.

- Theorem 1 does not require  $B$  to be symmetric, or even square;  $m < n$  is allowed. It does not apply directly to the  $m > n$  case, as the left null space  $V_0$  is larger than the rank deficiency of  $B$ .
- Finding a numerical null space of a matrix is a classical problem in numerical linear algebra, and a reliable algorithm is usually based on either the SVD or a strong rank-revealing QR factorization [42]. The assumptions in the theorem are much weaker; the reason they suffice is that (7) only states that the null space  $V_0$  is *contained* in (and not equal to)  $Q_2$ ; in particular, it does not claim  $\|BQ_2\|_2$  is small. Once such  $Q_2$  is obtained, our algorithm will extract a null space of  $BQ_2$  using the Rayleigh-Ritz process.

When Theorem 1 is applied with  $B \leftarrow r(\tilde{A}) + I$  as in (6) (so  $m = n$ ), it gives  $\sin \angle(V_0, Q_2) \leq \frac{\|V_0^*(r(\tilde{A})+I)\|_2}{\sigma_{\min}(R_{11})}$ , where  $V_0$  is the numerical null space of  $r(\tilde{A}) + I$ , which has dimension  $\geq k$  by construction. Therefore  $\|V_0^*(r(\tilde{A}) + I)\|_2 = O(u)$ , and it follows that we have  $\sin \angle(V_0, Q_2) \leq O(u/\sigma_{\min}(R_{11}))$ , so  $Q_2$  contains  $V_0$  to working accuracy provided that  $\sigma_{\min}(R_{11}) \geq \text{tol}$  for some tolerance  $\text{tol} = \Omega(1)$ , for example  $\text{tol} = 0.01$ , which is the choice we make by default. Choosing it too large,  $\text{tol} \approx 1$ , results in  $\ell \approx n$  so no computational savings, while  $\text{tol} \ll 1$  causes loss of accuracy.

**Choosing the subspace size  $\ell$**  We have seen that by looking for an  $\ell$  such that  $R_{11} \in \mathbb{C}^{(n-\ell) \times (n-\ell)}$  satisfies the condition  $\sigma_{\min}(R_{11}) \gtrsim \text{tol}$ , we can find a subspace  $Q_2 \in \mathbb{C}^{n \times \ell}$  that contains the desired subspace. We would like to find the smallest possible  $\ell$  to reduce the cost of the subsequent operations.

Fortunately, the condition  $\sigma_{\min}(R_{11}) \gtrsim \text{tol}$  can be checked reliably without computing the singular values of  $R_{11}$ . The key fact is that if (6) is a rank-revealing QR factorization, then the  $i$ th diagonal element of  $R_{11}$  is a good approximation to  $\sigma_i(R_{11})$  [43]. This more than suffices, given that violation by an  $O(1)$  factor in the condition  $\sigma_{\min}(R_{11}) \gtrsim \text{tol}$  only reduces the final accuracy by an  $O(1)$  factor. It follows that we can simply examine the diagonal entries of  $R$  in the QR factorization of  $r(\tilde{A}) + I$  to determine  $\ell$ .

In many cases, the QR factorization without pivoting is already rank revealing; if not, or to ensure this is true with high probability, one can take the QR of  $(r(\tilde{A}) + I)\Omega$  for an  $n \times n$  random Gaussian matrix  $\Omega$ —it is known that such

QR factorization is rank revealing with high probability [44]. (We can alternatively use QR with pivots, but this incurs substantial communication overhead in parallel computing settings.)

Once we have computed such a QR factorization, we look for the first diagonal  $(i, i)$ -element of  $R$  that comes below  $tol$ , and take  $i - 1$  to be the size of  $R_{11}$ , that is,  $\ell = n - i + 1$ .

Once  $Q_2$  is obtained, we then extract the desired space  $V_0$  from it by the Rayleigh-Ritz process: compute the eigenvalues of the  $\ell \times \ell$  matrix  $Q_2^* A Q_2$ , whose negative eigenvalues should match those of  $\Lambda_-$ . Denoting by  $Q_2^* A Q_2 = W \Lambda_- W^*$  the eigenvalue decomposition, the  $Q_2 W$  is the matrix of eigenvectors. By construction,  $Q_2^* A Q_2$  usually contains eigenvalues that are positive, and we discard those.  $W$  is then an  $\ell \times k$  matrix corresponding to the negative eigenvalues.

We note that since we are interested in extremal eigenvalues, Rayleigh-Ritz is a reliable means to extract the desired subspace.

**Choosing  $s$**  Let us consider in more detail the choice of the shift parameter  $s$ . The qualitative behavior has been explained already; taking  $s$  small results in the Zolotarev function being a poor approximant to  $\text{sign}(x)$  in the interval  $[-1, 0]$  that we care about, while a large  $s$  results in good approximation  $r(x) \approx -1$  on  $[-1, 0]$ , but (undesirably) also on a significant positive interval, resulting in the projected size being large.

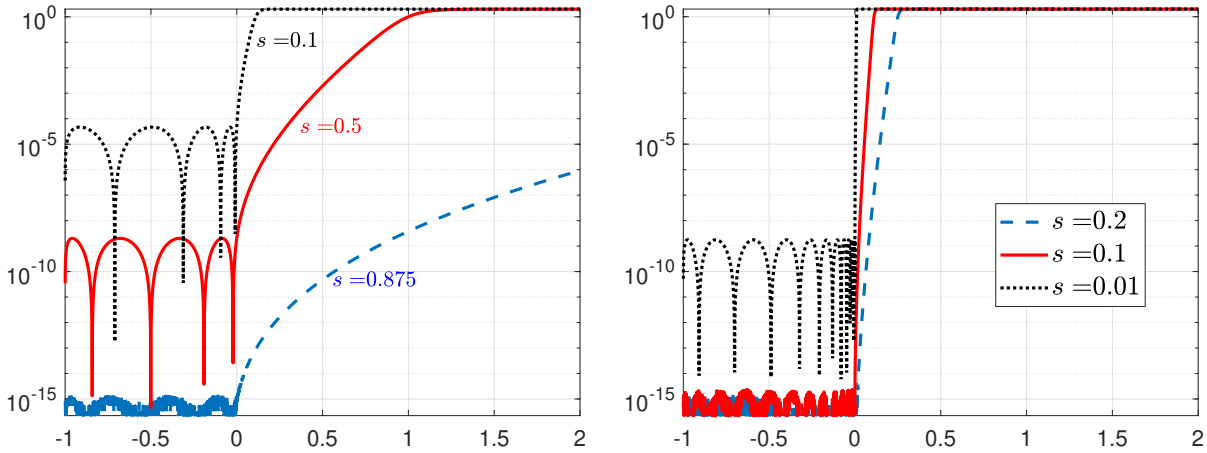


Figure 2: Semilogy plot of  $r(x - s) + 1$  for different choices of  $s$ , for Zolotarev functions of type  $(9, 8)$  (left) and  $(27, 26)$  (right).

We illustrate this in Fig. 2. For example, the left plot uses two QDWH iterations, so a Zolotarev function of type  $(9, 8)$ . Taking  $s = 0.875$  gives  $O(u)$  approximation quality on  $[-1, 0]$ , but the region in which  $r(x) + 1$  is close to 0 extends far into the positive axis. Taking  $s = 0.1$ , on the other hand, solves that issue, but the approximation quality on  $[-1, 0]$  is evidently worse. A similar behavior is seen on the right plot, where we use three QDWH iterations and hence a Zolotarev function of higher type  $(27, 26)$ . Here the essence stays the same, but a much smaller  $s$  is enough to obtain  $O(u)$  accuracy on  $[-1, 0]$ , and the functions  $r(x)$  grow steeply until  $\approx 1$  for  $x > 0$ .

Since the goal of the QDWHpartial-EIG iterations is to map the eigenvalues in  $[-1, 0]$  to 0 (to working precision  $O(u)$ ) by the rational function  $r(x) + 1$  while keeping the positive eigenvalues well separated from 0, the above observation leads to the following strategy for choosing  $s$ :

1. Determine the type  $(2m + 1, 2m)$  of rational function  $r(x)$  to be used.
2. Choose the smallest  $s$  so that  $|r(x) + 1| \leq O(u)$  on  $[-1, 0]$ .

In practice, the type  $(2m + 1, 2m)$  is chosen depending on the computational budget, and we shall mainly focus on two values  $2m + 1 = 3^2$  and  $2m + 1 = 3^3$ , as these lend to particularly efficient evaluation, by taking advantage of the optimality of Zolotarev functions under composition [41]. Specifically, they correspond to taking two ( $2m + 1 = 3^2$ ) and three ( $2m + 1 = 3^3$ ) QDWH iterations. For each choice, the value of  $s$  satisfying the second condition above is found (by simple experiments) to be

1. Type  $(9, 8)$ , two QDWH iterations:  $s = 0.875$ ,
2. Type  $(27, 26)$ , three QDWH iterations:  $s = 0.2$ .

These choices are shown in the two plots in Fig. 2. In most cases, taking three QDWH iterations is recommended as the overhead is not too much, while the benefit is significant, as can be seen clearly in Fig. 2: the function  $r(x) + 1$  of the corresponding cases ( $s = .875$  and  $s = 0.2$ ) take  $O(1)$  values for  $x \gtrsim 0.1$  with three QDWH iterations, but with two iterations, we require  $x \gtrsim 5$ . Consequently, the projected matrix size  $\ell$  will be approximately equal to the number of eigenvalues in  $[-1, 0.1]$  with three QDWH, but with two iterations, it captures eigenvalues in  $[-1, 5]$ , rendering QDWH<sub>partial</sub>-EIG useless unless there is a significant portion of large and positive eigenvalues in  $A$ . We therefore choose the default to be  $s = 0.2$  and three QDWH iterations. Note that in all iterations, one can safely use the fast Cholesky-based implementation in Eq. (3). Algorithm 1 presents the main computational steps of QDWH<sub>partial</sub>-EIG.

---

**Algorithm 1** QDWH<sub>partial</sub>-EIG. Given a symmetric or Hermitian matrix  $A$ , computes the negative eigenvalues and corresponding eigenvectors.

---

- 1: Find an approximate lower bound  $\mu \lesssim \lambda_{\min}(A) (< 0)$  using a few steps of the Lanczos algorithm, and set  $A := A/|\mu|$ .
  - 2: Set  $s = 0.2$  (or  $s = 0.875$ ) and apply three (or two) iterations of QDWH (using Eq. (3)) to  $\tilde{A} := (1 - s)A - sI$  with  $\ell_0 = s$ , to obtain  $r(\tilde{A})$  where  $r$  is of type  $(3^3, 3^3 - 1)$  (or type  $(3^2, 3^2 - 1)$ ).
  - 3: Compute the QR factorization  $\frac{1}{2}(r(\tilde{A}) + I) = QR$  (or  $\frac{1}{2}(r(\tilde{A}) + I)\Omega = QR$ , where  $\Omega$  is a Gaussian matrix).
  - 4: Find the index  $ind = \min(\text{find}(\text{abs}(\text{diag}(R)) < \text{tol} = 0.01))$ .
  - 5: Extract the final columns of  $Q$  to get  $Q_2 = Q(:, ind : \text{end})$ .
  - 6: Rayleigh-Ritz: Compute  $Q_2^* A Q_2$  and its eigenvalue decomposition  $Q_2^* A Q_2 = \tilde{V} \Lambda \tilde{V}^*$ . Extract the parts corresponding to the negative eigenvalues,  $\Lambda_-, \tilde{V}_-$ .
  - 7: Rescale  $\Lambda := |\mu| \Lambda_-$  and output  $\Lambda$  (negative eigenvalues) and  $V := Q_2 \tilde{V}_-$  (eigenvectors) such that  $AV \approx V\Lambda$ .
- 

Clearly, the algorithm is able to compute the positive eigenvalues, or those that are smaller or larger than a prescribed value by working with a shifted matrix  $A - cI$ .

## 4.2 QDWH<sub>partial</sub>-SVD

Given a general matrix  $A \in \mathbb{C}^{m \times n}$  ( $m \geq n$ ), we next consider the task of computing its dominant singular triplets, namely computing the singular values and singular vectors corresponding to the singular values above a given user-specified relative threshold  $s > 0$ ; we use the same letter as the shift for QDWH<sub>partial</sub>-EIG as they play a similar role.

As we shall see, essentially the same idea can be applied of optimizing the rational function only in the desired part. It is nonetheless worth noting that here we cannot use shifts, as to shift singular values without modifying the singular vectors we need the unitary polar factor, which is expensive to compute.

Assuming w.l.o.g. that  $\|A\|_2 \approx 1$  (this can be enforced using an inexpensive norm estimator  $\alpha \approx \|A\|_2$ , followed by a scaling  $A \leftarrow A/\alpha$ ), the idea is simply to compute  $r(A) := Ur(\Sigma)V^*$ , where  $r$  is a rational function that maps the interval  $[s, 1]$  to 1, to machine precision. The upshot is that if  $s \gg \sigma_{\min}(A)$ , then  $r$  is allowed to be of much lower degree than would be needed for computing  $U_p$ . See Fig. 3 for an illustration.

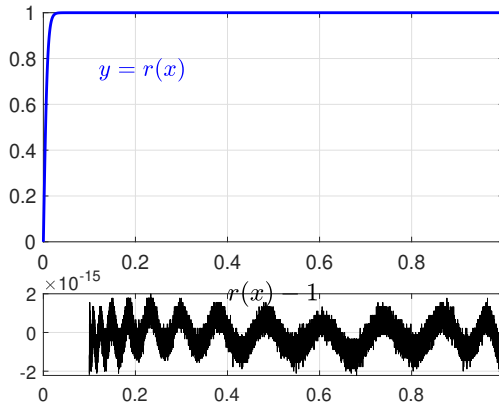


Figure 3: A type (27, 26) Zolotarev function  $r$  (top) that maps the interval  $[s, 1]$  to 1 for  $s = 0.1$ , and its the error  $r - 1$  (below). Note the error is  $O(u)$  on  $[s, 1]$ ; illustrating that three QDWH iterations is enough to find the singular values larger than  $s = 0.1$ .

It is worth noting that the degree of  $r$  and the number of QDWH iterations depend on the user-defined value  $s$ , unlike QDWH<sub>partial</sub>-EIG (for which  $s = 0.2$  is a “fixed” choice). Accordingly, if  $s \ll 1$  (say  $s < 10^{-3}$ ), for the first QDWH iteration it is advisable to use the QR-based implementation in Eq. (2) rather than Eq. (3) to avoid instabilities.

We also note that we use  $|\ell_k - 1| < O(u)$  as the stopping criterion for QDWH. This is because the standard condition, which requires convergence of  $X_k$ , is not necessarily satisfied when  $[s, 1]$  has been mapped to  $1 \pm O(u)$ , because the singular values  $\sigma_i(\tilde{A}) < s$  have not converged and lie somewhere in  $[0, 1]$ . (The situation was the same in QDWH<sub>partial</sub>-EIG, but there it was simpler as the iteration number is always three.)

Once  $r(A)$  is computed, one can find the desired column space  $U_1$  (leading columns of  $U$  corresponding to singular values of  $A$  larger than  $s$ ) by finding the null space of  $I - r(A)^*r(A)$ , which we do as before using the QR factorization (with randomization if needed) and looking for the diagonal entries of  $R$ . It is worth noting that computing the matrix  $r(A)^*r(A)$  may seem ill-advised, as it squares the condition number. This is not an issue here, as the quantity of interest is the singular subspace corresponding to the largest singular values of  $r(A)$  (which are  $\approx 1$ ).

Algorithm 2 gives a pseudocode of the overall algorithm.

---

**Algorithm 2** QDWH<sub>partial</sub>-SVD. Given  $A \in \mathbb{C}^{m \times n}$  ( $m \geq n$ ) and threshold  $s > 0$ , compute the singular values larger than  $s\|A\|_2$  and the corresponding singular vectors.

---

- 1: Estimate  $\alpha \approx \|A\|_2$  with a norm estimator.
  - 2: Apply QDWH to  $\tilde{A} := A/\alpha$  with  $\ell_0 = s$  until  $|\ell_k - 1| < O(u)$  to obtain  $r(\tilde{A})$ .
  - 3: Calculate  $[Q \ R] = QR(I - r(\tilde{A})^*r(\tilde{A}))$ .
  - 4: Find the index  $ind = \min(\text{find}(\text{abs}(\text{diag}(R)) < \text{tol} = 0.01))$ .
  - 5: Extract  $Q_2 = Q(:, ind : \text{end})$ .
  - 6: Projection: Compute  $AQ_2$  and its SVD  $AQ_2 = \tilde{U}\tilde{\Sigma}\tilde{V}^*$ .
  - 7: Extract the singular triplets with singular values larger than  $s\|A\|_2$ , call them  $\tilde{U}_1, \tilde{\Sigma}_1, \tilde{V}_1$ .
  - 8: Let  $U_1 := \tilde{U}_1, \Sigma_1 := \tilde{\Sigma}_1$  and  $V_1 := Q\tilde{V}_1$ .
- 

The outputs of QDWH<sub>partial</sub>-SVD are  $U_1, \Sigma_1, V_1^*$  such that  $U_1\Sigma_1V_1^*$  is the truncated SVD of  $A$ , truncated at the first singular value smaller than  $s$ .

The computational savings comes from the fact that  $AQ_2$  is much thinner than  $A$ ; the number of columns of  $AQ_2$  is slightly more than the number of singular values of  $A$  larger than  $s$ .

Of course, if  $m < n$  one can simply apply the algorithm to  $A^*$ .

## 5 Implementation details

The main basic blocks of QDWH<sub>partial</sub>-EIG in Algorithm 1 correspond to a subset of QDWH<sub>partial</sub>-SVD operations, as shown in in Algorithm 2. Therefore, we only provide implementation details of QDWH<sub>partial</sub>-SVD. Algorithm 3 describes the pseudo-code of the distributed-memory implementation of QDWH<sub>partial</sub>-SVD based on ScaLAPACK [16].

Following the 2D Block-Cyclic Data Distribution (2D-BCDD) used in ScaLAPACK, we define the MPI process grid configuration as  $P \times Q$ . Each data structure owns a handle or a descriptor that expresses how the data structure is distributed following the 2D-BCCD. ScaLAPACK relies on the Basic Linear Algebra Communication Subprograms (BLACS) library, which is in charge of performing data movements during the matrix computations through the traditional MPI. ScaLAPACK relies on block algorithms, which can be expressed by two successive computational stages: the panel factorization and the update of the trailing submatrix. While the former is memory-bound, and typically sequential and may not benefit from having many processors participating, the latter is rich in compute-bound operations. This is where most of ScaLAPACK dense linear algebra operations extract parallel performance by means of calls to Level-3 BLAS, as implemented in the Parallel BLAS (PBLAS) layer. The blocking size referred as  $nb$  is an internal tuning parameter that trades-off the degree of parallelism and the performance of the computational kernels. Moreover, the number of processors should be properly calibrated into a rectangular shape with  $Q > 1.5P$  to carry on, in parallel, the update of the trailing submatrix.

As shown in Algorithm 3, the QDWH<sub>partial</sub>-SVD code is mostly composed of conventional dense linear algebra matrix kernels rich in compute-intensive Level-3 BLAS operations that are capable of achieving a decent percentage of the system’s theoretical peak performance. Since these matrix kernels are widely available in vendor optimized numerical libraries, porting to various hardware architectures should not be cumbersome. The code is written in double precision arithmetics, and can be extended to other precisions for a broader application coverage.

---

**Algorithm 3** Pseudo-code of the QDWHpartial-SVD using ScaLAPACK.
 

---

```

/* Set block size and initiate CBLACS context */
1: Cblacs_get(0, 0, ictxt)
2: Cblacs_gridmap(ictxt, imap, P, P, Q)
3: Cblacs_gridinfo(ictxt, P, Q, myrow, mycol)
4: /* Initialize data structures using the 2D-BCDD descinit() */
5: descinit(nb, nb, A, descA); Fill_in(A, descA)
/* Estimate the two-norm of the matrix */
6:  $\alpha = \text{pdggenm2}(A)$ 
7:  $\text{pdlascl}(\alpha, 1., A)$ 
/* Computing the polar factor  $U_p$  of the matrix  $A$  using QDWH */
8:  $k = 1$ ,  $Li = \text{threshold}(s)$ ,  $conv = 100$ 
9: while ( $|Li - 1| \geq 5\text{eps}$ ) do
10:  $L2 = Li^2$ ,  $dd = \sqrt[3]{(4(1 - L2)/L2^2)}$ 
11:  $sqd = \sqrt{1 + dd}$ 
12:  $a1 = sqd + \sqrt{8 - 4 \times dd + 8(2 - L2)/(L2 \times sqd)}/2$ 
13:  $a = \text{real}(a1)$ ;  $b = (a - 1)^2/4$ ;  $c = a + b - 1$ 
14:  $Li = Li(a + b \times L2)/(1 + cL2)$ 
15:  $\text{pdlacpy}(U, U1)$ 
16: /* Compute  $U_k$  from  $U_{k-1}$  */
17:  $\text{pdlaset}(Z, 0., 1.)$ 
18:  $\text{pdgemm}(U^T, U, Z)$ 
19:  $\text{pdgeadd}(U, B)$ 
20:  $\text{pdposv}(Z, B)$ 
21:  $\text{pdgeadd}(B, U)$ 
22:  $\text{pdgeadd}(U, U1)$ 
23:  $\text{pdlange}(U1, conv)$ 
24:  $k = k + 1$ 
25: end while
/*  $U_p$  contains the isolated subspectrum of interests */
26:  $\text{pdlaset}(0.0, 1.0, B)$ 
27:  $\text{pdgemm}(U_p^T, U_p, B)$ 
28:  $\text{pdgeqrf}(B)$ 
29:  $ind = \min(\text{find}(\text{abs}(\text{diag}(B)) < \text{tol} = 0.01))$ 
30:  $\text{pdorgqr}(B, Q)$ 
/*  $\text{size}(\tilde{A}) = N - ind$  */
31:  $Q_2 = Q(:, ind:end)$ 
32:  $\text{pdgemm}(A, Q_2, \tilde{A})$ 
/* Calculate the SVD on the reduced problem */
33:  $\text{pdgesvd}(\tilde{A}, \tilde{U}, \tilde{\Sigma}, \tilde{V})$ 
/*  $\tilde{U}_1, \tilde{\Sigma}_1, \tilde{V}_1$  are the singular triplets with singular values larger than the  $s \times \alpha$  */
34:  $U = \tilde{U}_1$ 
35:  $\Sigma = \tilde{\Sigma}_1$ 
36:  $\text{pdgemm}(\tilde{V}_1, Q_2^T, V)$ 

```

---

## 6 Operation counts

Table 1 reports the operation counts of various symmetric EIG and SVD solvers on square matrices of size  $n$ : the PDSYEVD / PDGESVD and QDWH-EIG / QDWH-SVD routines for computing the full spectrum and the QDWHpartial-EIG / QDWHpartial-SVD routines for computing a subset of the spectrum. We refer the reader to [20] for further details on the costs of the standard and QDWH-based EIG / SVD solvers.

The operation counts of QDWHpartial-EIG and QDWHpartial-SVD depends on the number of Cholesky-based QDWH iterations (typically two or three) and, the QR, GEMM and SYRK to form the reduced problem matrix of size  $N_s \geq s$ , with  $s$  the size of the partial spectrum of interest. The actual full EIG and SVD occurs now only on the reduced problem matrix of size  $N_s$ . Assuming  $N_s \ll N$  and three Cholesky-based iterations to get the polar factor from QDWH, the total number of operations is up to  $14N^3$  and  $24N^3$  for QDWHpartial-EIG ( $it_{Chol} = 3$ ) and QDWHpartial-SVD ( $it_{QR} = 1$  and  $it_{Chol} = 3$ ), respectively.

## 7 Numerical accuracy

The numerical accuracy of the QDWH-based algorithms to compute the polar decomposition, the eigenvalue decomposition (QDWH-EIG) and singular value decomposition (QDWH-SVD) have been verified in [20]. The robustness of their high performance implementations has been studied on shared-memory systems [21] and on distributed-memory systems [22, 23]. In this Section, we present the numerical robustness of the QDWHpartial-EIG and QDWHpartial-SVD implementations on distributed-memory system.

EIG and SVD variants	Cost
Standard full EIG	$9N^3$
Full QDWH-EIG	$(17 + \frac{4}{9})N^3 \leq \dots \leq (52 + \frac{1}{9})N^3$
QDWHpartial-EIG	QDWH: $(4+1/3)N^3 \times \#it_{Chol}$ QR + SYRK + GEMM: $4/3N^3 + N_s N^2 + 2N_s^2 N$ EIG: $9N_s^3$
Standard full SVD	$17N^3$
Full QDWH-SVD	$20N^3 \leq \dots \leq (50 + \frac{1}{3})N^3$
QDWHpartial-SVD	QDWH: $(8+2/3)N^3 \times \#it_{QR} + (4+1/3)N^3 \times \#it_{Chol}$ QR + SYRK + 2×GEMM: $4/3N^3 + N^3 + 4N_s N_s^2$ SVD: $17N_s^3$

Table 1: Operation counts for various symmetric EIG and SVD algorithms.

## 7.1 Environment Settings

We run our experiments on a Cray XC40 system codenamed *Shaheen-2* installed at the KAUST Supercomputing Laboratory (KSL), with the Cray Aries network interconnect, which implements a Dragonfly network topology. The system has 6174 compute nodes, each with two-socket 16-core Intel Haswell running at 2.3GHz and 128GB of DDR3 main memory. The Haswell nodes on *Shaheen-2* have a theoretical peak performance of approximately 1.18 TFlops/s. Furthermore, “hugepages” are employed to improve memory accesses. The work load managers on *Shaheen-2* is native SLURM. We use the Intel compiler v15.0.2.164. We rely on the ScaLAPACK implementation from the high performance Cray LibSci numerical library, which depends on the MPI programming model for inter-node communications.

All runs for a given process configuration have been submitted in the same job submission script to reduce the impact from the system jitter. All the experiments are performed using IEEE double-precision arithmetic.

## 7.2 Synthetic Matrices

The dense synthetic matrices  $A \in \mathbb{R}^{N \times N}$  are generated using the ScaLAPACK routine PDLATMS  $A = Q_1 D Q_2^\top$  with setting mode = 0. For the symmetric EIG solvers testing, the matrices are generated with an equispaced eigenvalues as follows:

$$D = \left\{ \begin{array}{ll} D[i] = & -k \times randn[i], \quad i \leq k \\ D[i] = & N - k \times randn[i], \quad i \geq k \end{array} \right\},$$

where  $k$  is the number of the negative eigenvalues. For the SVD solvers testing, the distribution of the singular values of the generated matrices follows a geometrical series:  $D[i] = (0.5)^{\frac{i}{N} * 100}$ . We compute then orthogonal matrices  $Q_1$  and  $Q_2$  generated by calculating the  $QR$  factorization of arbitrary matrices to form the SVD, while  $Q_1 = Q_2$  for the symmetric EIG solvers. The performance of the matrix generation step may be expensive and can be improved but this is beyond the scope of this paper.

## 7.3 Norm Definitions

For a given general matrix  $A \in \mathbb{R}^{N \times N}$ , let  $\Sigma = diag(\sigma_1, \sigma_2, \dots, \sigma_k)$  be the  $k$  computed singular values, and  $U$  and  $V$  be the corresponding  $k$  computed left and right singular vectors. The norm  $\| \cdot \|_F$  denotes the Frobenius norm. The accuracy assessment of the partial computation of the SVD are based on the following metrics:

$$\frac{\|I - UU^\top\|_F}{n} \quad \text{and} \quad \frac{\|I - VV^\top\|_F}{n}, \quad (8)$$

for the orthogonality of the left and right  $k$  computed singular vectors  $U$  and  $V$ , respectively, and

$$\frac{\|\Sigma - \Delta\|_F}{\|\Delta\|_F}, \quad (9)$$

for the accuracy of the  $k$  computed singular values  $\Sigma$ , where  $\Delta$  is the  $k$  exact singular values (analytically known), and

$$\max_i (\|AU(:, i) - \sigma_i V(:, i)\|_F) \quad \text{and} \quad \max_i (\|AV(:, i) - \sigma_i U(:, i)\|_F) \quad (10)$$

for the accuracy of the left and right singular value decomposition, respectively. Similarly, for a symmetric matrix  $A \in \mathbb{R}^{n \times n}$ , the accuracy of the computed  $k$  negative eigenvalues, the orthogonality of their corresponding eigenvectors and the overall residual can be accordingly measured using 8, 9 and 10, respectively.

#### 7.4 Accuracy Assessments of EIG/SVD Solvers

This section highlights the numerical robustness of QDWH<sub>partial</sub>-SVD and QDWH<sub>partial</sub>-EIG implementations. Fig. 4 (a, b, c) shows the numerical accuracy of the computed singular values (Equation 9), the orthogonality of their corresponding singular vectors (Equation 8) and the right/left residual of the computed SVD (Equation 10) on a  $16 \times 36$  grid configuration (similar accuracy results for larger grid sizes  $32 \times 72$ ,  $64 \times 144$  and  $128 \times 288$ ) using synthetic ill-conditioned matrices. Herein, we compare the accuracy of three implementations of the SVD solvers: QDWH<sub>partial</sub>-SVD (setting different threshold  $s$ ) against PDGESVD from ScaLAPACK and from KSVD<sup>4</sup> [23]. The QDWH<sub>partial</sub>-SVD is capable to extract only the singular values/vectors of interest within the user-defined threshold  $s$ . This threshold  $s$  can be tuned with *a priori* knowledge on the singular value distribution (e.g., globally low-rank structure). This tunable parameter can directly influence the number of the computed singular values/vectors. For instance, in Fig. 4 (a, b, c), we study the accuracy for  $s = 0.1, 0.01, 0.001, 0.0001$  that translates into the percentages 3%, 7%, 10%, 13% of the computed singular values/vectors, respectively, and as a result affect the performance of QDWH<sub>partial</sub>-SVD. It is noteworthy that the ScaLAPACK PDGESVD computes first the whole SVD, then the requested singular values/vectors are filtered out using the threshold parameter  $s$ .

Figures 4 (d, e, f) shows the numerical accuracy of three different EIG solvers to compute 10% of the negative eigenvalues: ELPA divide-and-conquer routine, ScaLAPACK PDSYEVD and QDWH<sub>partial</sub>-EIG. ELPA and QDWH<sub>partial</sub>-EIG are capable of computing a fraction of the negative eigenspectrum. The ScaLAPACK PDSYEVD calculates first the entire eigenspectrum and then only the 10% of the negative eigenspectrum are selected.

These extensive numerical tests in Fig. 4 demonstrate the numerical robustness of QDWH<sub>partial</sub>-SVD and QDWH<sub>partial</sub>-EIG to provide satisfactory accuracy up to the machine precision for double precision computations across all studied matrix sizes.

## 8 Performance results

Figure 5 highlights the performance comparisons of QDWH<sub>partial</sub>-SVD against the two other SVD solvers, ScaLAPACK PDGESVD and KSVD [23] across various matrix sizes and process grid configurations. When only 13% of the spectrum is needed, QDWH<sub>partial</sub>-SVD achieves performance superiority as we increase the matrix sizes up to  $[6.3X, 2X]$  on  $16 \times 36$ ,  $[6X, 2X]$  on  $32 \times 72$ ,  $[3.3X, 2.3X]$  on  $64 \times 144$  and  $[4X, 1.8X]$  on  $128 \times 288$  grid topologies against [ScaLAPACK PDGESVD, KSVD], respectively. Moreover, on  $16 \times 36$  grid configuration, QDWH<sub>partial</sub>-SVD achieves similar performance when only 13%-10%-7% of the spectrum is needed, since the QDWH-based polar decomposition is the most time consuming step. We observe a slightly faster time to solution though, when only 3% of the spectrum is calculated, since the size of the reduced problem maybe relatively smaller than the aforementioned partial spectrums.

Fig. 6 reports the performance comparisons of QDWH<sub>partial</sub>-EIG against the two other EIG solvers, ScaLAPACK PDSYEVD and ELPA across various matrix sizes and process grid configurations. QDWH<sub>partial</sub>-EIG achieves performance superiority as we increase the matrix sizes up to  $1.5X$  on  $16 \times 36$ ,  $1.3X$  on  $32 \times 72$ ,  $1.6X$  on  $64 \times 144$  and  $3.5X$  on  $128 \times 288$  grid topologies against ScaLAPACK PDSYEVD. QDWH<sub>partial</sub>-EIG remains slower than the two-stage approach of ELPA. However, QDWH<sub>partial</sub>-EIG exposes more parallelism throughout the execution than ELPA (i.e., the reduction from band to tridiagonal form is limited in parallelism). As we increase the number of processors, QDWH<sub>partial</sub>-EIG is more capable of extracting performance from the underlying hardware architecture than ELPA.

Indeed, Fig. 7 shows the sustained performance in Tflops/s and explains why the the performance gap between QDWH<sub>partial</sub>-EIG and ELPA gets narrower. As we increase the matrix sizes and the process grids, QDWH<sub>partial</sub>-EIG obtains up to a twice higher rate of executions than ELPA. This performance efficiency may become an advantage moving forward with a hardware landscape oriented toward massively parallel resources delivering high rate of executions (e.g., accelerator-based supercomputers).

Figure 8 shows various grid topologies and indicates a decent performance scalability of QDWH<sub>partial</sub>-SVD and QDWH<sub>partial</sub>-EIG, as the matrix sizes increases. Notice also the various slopes flatten for both solvers, since the critical computational phase, i.e., the QDWH-based polar decomposition, enters into the compute-bound regime of operations along with a better hardware occupancy. It is also noteworthy to emphasize that the size of the reduced

<sup>4</sup>Available at <https://github.com/ecrc/ksvd>

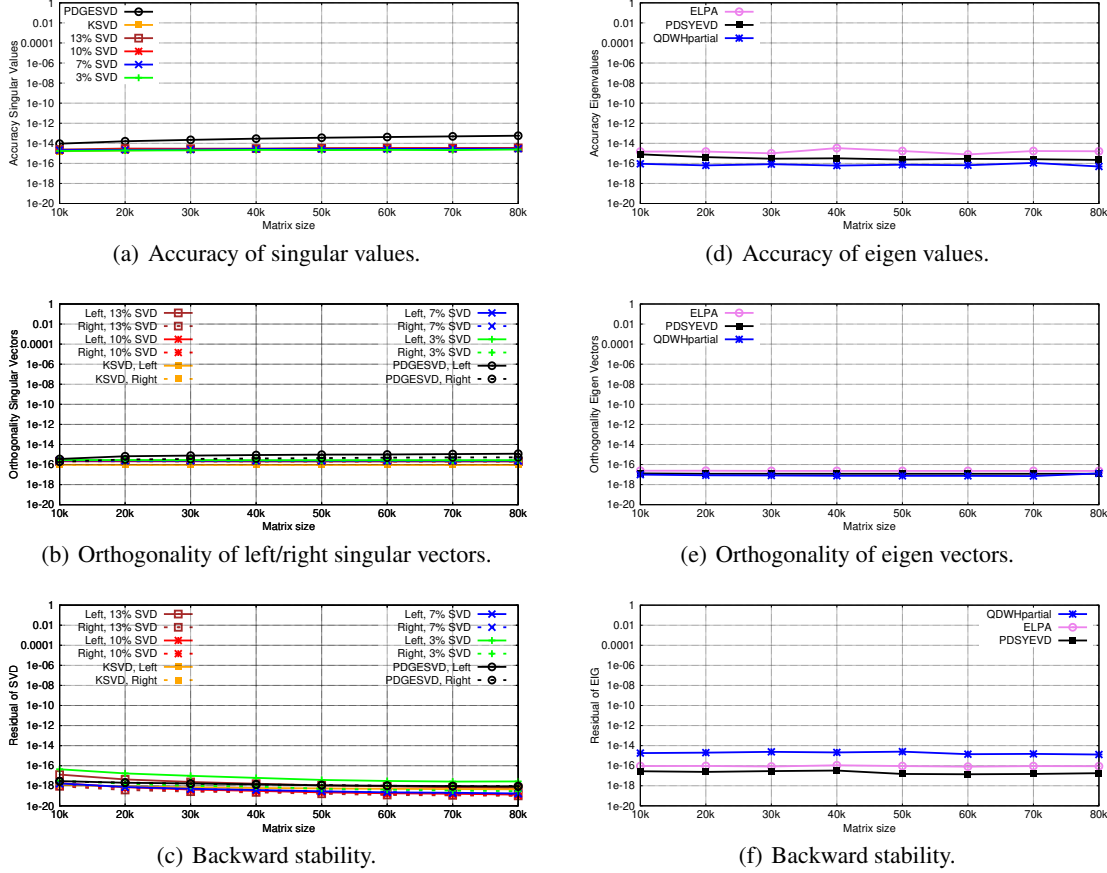
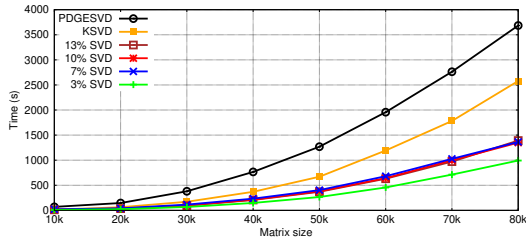


Figure 4: Assessing the numerical accuracy/robustness using  $16 \times 36$  grid topology: (a-b-c) for SVD solvers and (d-e-f) for EIG solvers

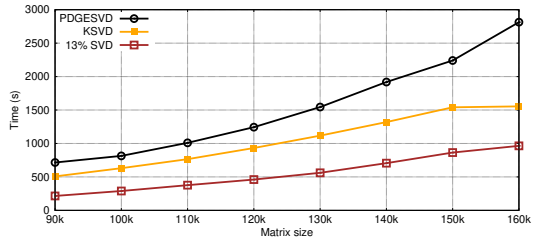
problem may sometimes be higher than the number of eigenvalues or singular values requested. This situation explains why QDWHpartial-EIG is sometimes faster than QDWHpartial-SVD, although their algorithmic complexities are comparable (see Table 1 in Section 6).

## 9 Summary and future work

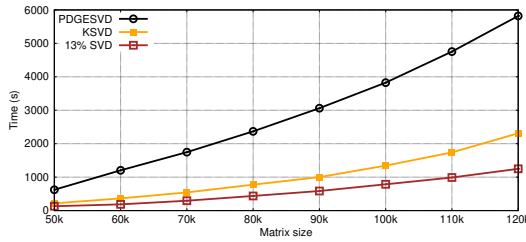
This paper introduces a new algorithm for computing a partial spectrum for the dense symmetric EIG and SVD solvers. By relying on QDWH-based polar decomposition, we demonstrate the numerical robustness of QDWHpartial-SVD and QDWHpartial-EIG against their counterpart routines from state-of-the-art open-source (i.e., ELPA and KSVD) and vendor-optimized (i.e., ScaLAPACK from Cray Scientific Library) numerical libraries. While QDWHpartial-SVD outperforms the existing approaches up to  $6X$ , QDWHpartial-EIG shows performance superiority up to  $3.5X$  against the one-stage approach of *PDSYEVD* from ScaLAPACK but remains slower compared to ELPA. We believe that the inherent massively parallel and compute-bound regime of QDWHpartial-EIG may help in narrowing the performance gap observed against ELPA moving forward with hardware rich in concurrency. We plan to further improve our current implementation by using *ZOLO*-based polar decomposition [45]. Recent work on leveraging task-based programming model associated with dynamic runtime systems for tackling heterogeneous hardware environment [36] may also be considered to further speed up the current implementation on distributed-memory systems equipped with GPU accelerators.



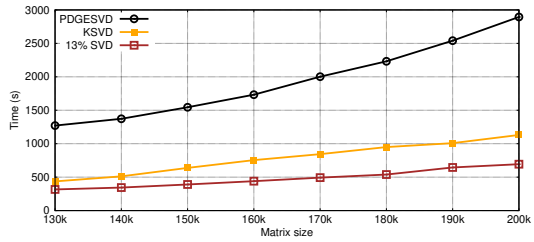
(a) P=16 and Q=36.



(c) P=64 and Q=144.

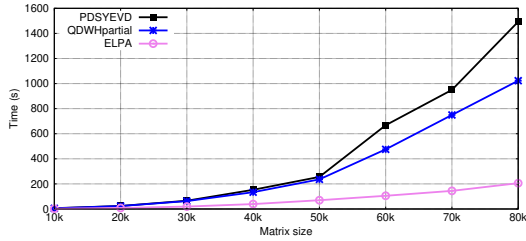


(b) P=32 and Q=72.

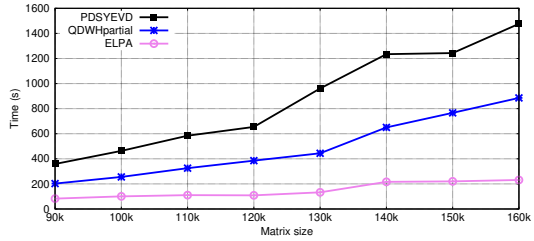


(d) P=128 and Q=288.

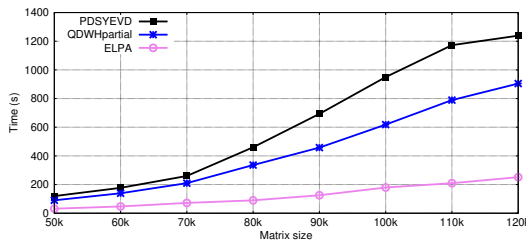
Figure 5: Performance comparisons in seconds of SVD solvers for various grid topologies.



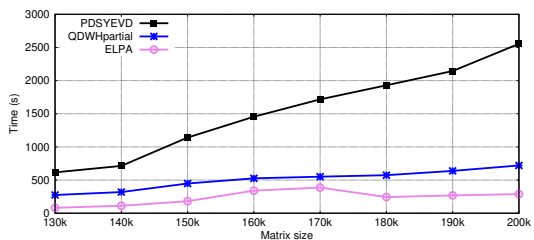
(a) P=16 and Q=36.



(c) P=64 and Q=144.



(b) P=32 and Q=72.



(d) P=128 and Q=288.

Figure 6: Performance comparisons in seconds of EIG solvers for various grid topologies.

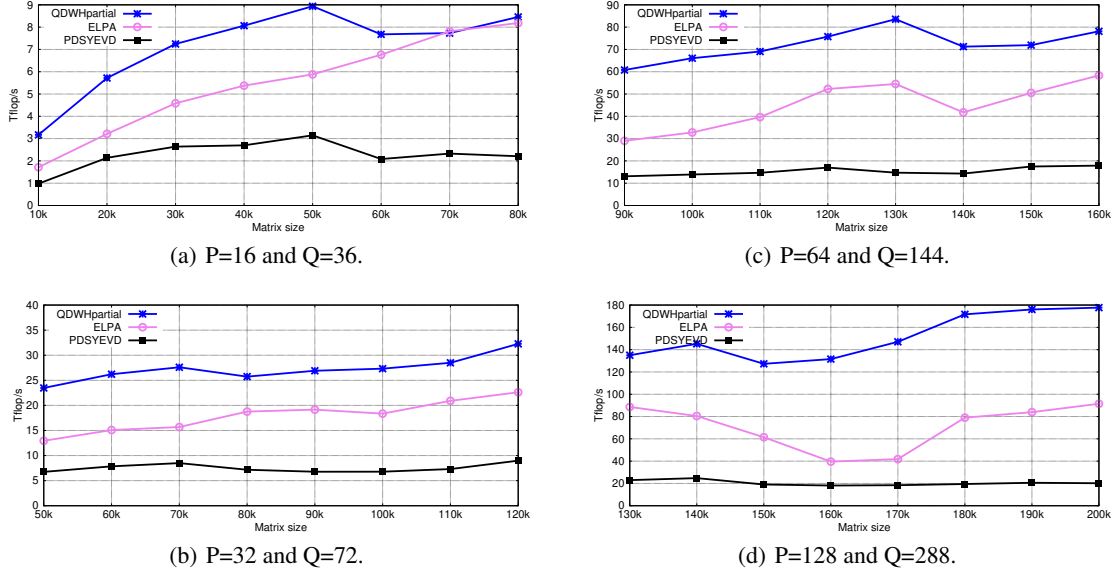


Figure 7: Performance comparisons in Tflops/s of symmetric EIG solvers for various grid topologies.

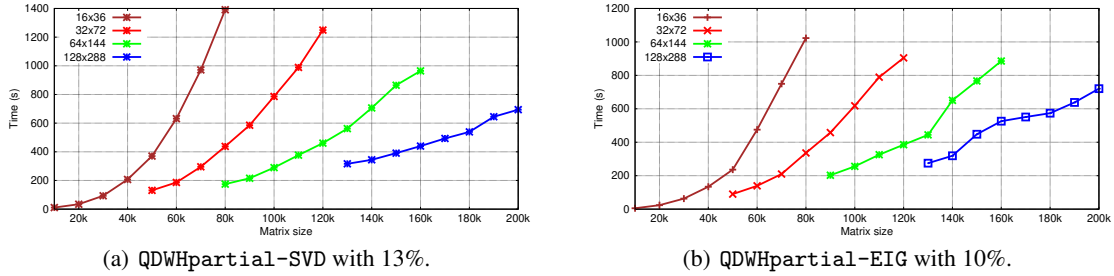


Figure 8: Performance scalability of QDWHpartial-SVD and QDWHpartial-EIG for various grid topologies.

## Acknowledgment

The authors would like to thank Cray Inc. and Intel in the context of the Cray Center of Excellence and Intel Parallel Computing Center awarded to ECRC at KAUST. For computer time, this research used *Shaheen-2* supercomputer hosted at the Supercomputing Laboratory at KAUST.

## References

- [1] Gene H. Golub and C. Reinsch. Singular Value Decomposition and Least Squares Solutions. *Numerische Mathematik*, 14:403–420, 1970.
- [2] Gene H. Golub and Charles F. Van Loan. *Matrix Computations*. The Johns Hopkins University Press, 4th edition, 2012.
- [3] Lloyd N. Trefethen and David Bau. *Numerical Linear Algebra*. SIAM, Philadelphia, PA, 1997.
- [4] Rémi Soummer, Laurent Pueyo, and James Larkin. Detection and characterization of exoplanets and disks using projections on karhunen-loève eigenimages. *The Astrophysical Journal Letters*, 755(2):L28, 2012.
- [5] Lars Eldén. *Matrix Methods in Data Mining and Pattern Recognition*. Fundamentals of algorithms. Society for Industrial and Applied Mathematics, pub-SIAM:adr, 2007.
- [6] I. V. Oseledets and E. E. Tyrtyshnikov. Breaking the Curse of Dimensionality, Or How to Use SVD in Many Dimensions. *SIAM J. Sci. Comput.*, 31(5):3744–3759, October 2009.
- [7] Notker Rösch, Sven Krüger, Vladimir A. Nasluzov, and Alexei V. Matveev. ParaGauss: The Density Functional Program ParaGauss for Complex Systems in Chemistry. In Arndt Bode and Franz Durst, editors, *High*

- Performance Computing in Science and Engineering, Garching 2004*, pages 285–296, Berlin, Heidelberg, 2005. Springer Berlin Heidelberg.
- [8] Dr Matt Probert. Electronic Structure: Basic Theory and Practical Methods, by Richard M. Martin. *Contemporary Physics*, 52(1):77–77, 2011.
- [9] Roger Grimes, Henry Krakauer, John Lewis, Horst Simon, and Su-Hai Wei. The solution of large dense generalized eigenvalue problems on the Cray X-MP/24 with SSD. *Journal of Computational Physics*, 69(2):471 – 481, 1987.
- [10] Y. Saad, A. Stathopoulos, J. Chelikowsky, K. Wu, and S. Ögüt. Solution of Large Eigenvalue Problems in Electronic Structure Calculations. *BIT Numerical Mathematics*, 36(3):563–578, Sep 1996.
- [11] Hatem Ltaief, Dalal Sukkari, Oliver Guyon, and David Keyes. Extreme Computing for Extreme Adaptive Optics: The Key to Finding Life Outside Our Solar System. In *Proceedings of the Platform for Advanced Scientific Computing Conference, PASC’18*, pages 1:1–1:10, New York, NY, USA, 2018. ACM.
- [12] Kadir Akbudak, Hatem Ltaief, Aleksandr Mikhalev, Ali Charara, Aniello Esposito, and David Keyes. Exploiting Data Sparsity for Large-Scale Matrix Computations. In *European Conference on Parallel Processing*, volume 11014. Springer, 2018.
- [13] Patrick Amestoy, Cleve Ashcraft, Olivier Boiteau, Alfredo Buttari, Jean-Yves L’Excellent, and Clément Weisbecker. Improving Multifrontal Methods by Means of Block Low-Rank Representations. *SIAM Journal on Scientific Computing*, 37(3):A1451–A1474, 2015.
- [14] Wolfgang Hackbusch. *Hierarchical Matrices: Algorithms and Analysis*, volume 49. Springer, 2015.
- [15] Edward Anderson, Zhaojun Bai, Christian Heinrich Bischof, Laura Susan Blackford, James Weldon Demmel, Jack J Dongarra, Jeremy J Du Croz, Anne Greenbaum, Sven Hammarling, A McKenney, and Danny C Sorensen. *LAPACK User’s Guide*. SIAM, Philadelphia, 3rd edition, 1999.
- [16] L. Suzan Blackford, J. Choi, Andy Cleary, Eduardo F. D’Azevedo, James W. Demmel, Inderjit S. Dhillon, Jack J. Dongarra, Sven Hammarling, Greg Henry, Antoine Petitet, Ken Stanley, David W. Walker, and R. Clint Whaley. *ScaLAPACK Users’ Guide*. Society for Industrial and Applied Mathematics, Philadelphia, 1997.
- [17] Bruno Lang. Efficient Eigenvalue and Singular Value Computations On Shared Memory Machines. *Parallel Computing*, 25(7):845–860, 1999.
- [18] Christian H. Bischof, Bruno Lang, and Xiaobai Sun. Algorithm 807: The SBR Toolbox—Software for Successive Band Reduction. *ACM Transactions on Mathematical Software*, 26(4):602–616, 2000.
- [19] Yuji Nakatsukasa, Zhaojun Bai, and Francois Gygi. Optimizing Halley’s Iteration for Computing the Matrix Polar Decomposition. *SIAM Journal on Matrix Analysis and Applications*, pages 2700–2720, 2010.
- [20] Yuji Nakatsukasa and Nicholas J. Higham. Stable and Efficient Spectral Divide and Conquer Algorithms for the Symmetric Eigenvalue Decomposition and the SVD. *SIAM Journal on Scientific Computing*, 35(3):A1325–A1349, 2013.
- [21] Dalal Sukkari, Hatem Ltaief, and David E. Keyes. A High Performance QDWH-SVD Solver Using Hardware Accelerators. *ACM Trans. Math. Softw.*, 43(1):6:1–6:25, 2016.
- [22] Dalal Sukkari, Hatem Ltaief, and David E. Keyes. High Performance Polar Decomposition on Distributed Memory Systems. In Pierre-François Dutot and Denis Trystram, editors, *Euro-Par 2016: Parallel Processing - 22nd International Conference on Parallel and Distributed Computing, Grenoble, France, August 24-26, 2016, Proceedings*, volume 9833 of *Lecture Notes in Computer Science*, pages 605–616. Springer, 2016.
- [23] Dalal Sukkari, Hatem Ltaief, Aniello Esposito, and David Keyes. A QDWH-Based SVD Software Framework on Distributed-Memory Manycore Systems. *ACM Trans. Math. Softw.*, 45(2), April 2019.
- [24] A. Marek, V. Blum, R. Johanni, V. Havu, B. Lang, T. Auckenthaler, A. Heinecke, H.J. Bungartz, and H. Lederer. The ELPA Library: Scalable Parallel Eigenvalue Solutions for Electronic Structure Theory and Computational Science. *J Phys Condens Matter*, 26(21), 2014.
- [25] Piotr Luszczek, Hatem Ltaief, and Jack Dongarra. Two-Stage Tridiagonal Reduction for Dense Symmetric Matrices using Tile Algorithms on Multicore Architectures. In *Proceedings of IPDPS 2011*, Anchorage, AK USA, 2011. ACM.
- [26] Azzam Haidar, Hatem Ltaief, and Jack Dongarra. Parallel Reduction to Condensed Forms for Symmetric Eigenvalue Problems Using Aggregated Fine-grained And Memory-aware Kernels. In *Proceedings of SC’11 Conference on High Performance Computing Networking, Storage and Analysis*, page 8, Seattle, WA, USA, November 2011. ACM SIGARCH/IEEE Computer Society.

- [27] A. Haidar, H. Ltaief, and J. Dongarra. Toward a High Performance Tile Divide and Conquer Algorithm for the Dense Symmetric Eigenvalue Problem. *SIAM Journal on Scientific Computing*, 34(6):249–274, 2012.
- [28] Hatem Ltaief, Piotr Luszczek, Azzam Haidar, and Jack Dongarra. Solving the Generalized Symmetric Eigenvalue Problem using Tile Algorithms on Multicore Architectures. In Koen De Bosschere, Erik H. D’Hollander, Gerhard R. Joubert, David A. Padua, Frans J. Peters, and Mark Sawyer, editors, *PARCO*, volume 22 of *Advances in Parallel Computing*, pages 397–404. IOS Press, 2011.
- [29] H. Ltaief, P. Luszczek, and J. Dongarra. Enhancing Parallelism of Tile Bidiagonal Transformation on Multicore Architectures using Tree Reduction. *International Conference on Parallel Processing and Applied Mathematics*, May 2011.
- [30] H. Ltaief, P. Luszczek, and J. Dongarra. High Performance Bidiagonal Reduction using Tile Algorithms on Homogeneous Multicore Architectures. *ACM Transactions on Mathematical Software*, 39(3), 2012.
- [31] Azzam Haidar, Stanimire Tomov, Jack Dongarra, Raffaele Solcá, and Thomas Schulthess. A Novel Hybrid CPU-GPU Generalized Eigensolver for Electronic Structure Calculations Based on Fine-Grained Memory Aware Tasks. *The International Journal of High Performance Computing Applications*, 28(2):196–209, 2014.
- [32] T. Fukaya and T. Imamura. Performance Evaluation of the Eigen Exa Eigensolver on Oakleaf-FX: Tridiagonalization Versus Pentadiagonalization. In *2015 IEEE International Parallel and Distributed Processing Symposium Workshop*, pages 960–969, May 2015.
- [33] Osni Marques, James Demmel, and Paulo B. Vasconcelos. Bidiagonal SVD Computation via an Associated Tridiagonal Eigenproblem. *ACM Trans. Math. Softw.*, 46(2), May 2020.
- [34] Nathan Halko, Per-Gunnar Martinsson, and Joel A Tropp. Finding structure with randomness: Probabilistic algorithms for constructing approximate matrix decompositions. 53(2):217–288, 2011.
- [35] Yuji Nakatsukasa. Fast and stable randomized low-rank matrix approximation. *arXiv:2009.11392*, 2020.
- [36] D. Sukkari, H. Ltaief, M. Faverge, and D. Keyes. Asynchronous Task-Based Polar Decomposition on Single Node Manycore Architectures. *IEEE Transactions on Parallel and Distributed Systems*, PP(99):1–1, 2017.
- [37] I.Y. Bar-Itzhack. Iterative Optimal Orthogonalization of the Strapdown Matrix. *Aerospace and Electronic Systems, IEEE Trans. on*, AES-11(1):30–37, Jan 1975.
- [38] Jerome A. Goldstein and Mel Levy. Linear Algebra and Quantum Chemistry. *Am. Math. Monthly*, 98(10):710–718, October 1991.
- [39] Robert Schreiber and Beresford Parlett. Block Reflectors: Theory and Computation. *SIAM Journal on Numerical Analysis*, 25(1):189–205, 1988.
- [40] Nicholas J. Higham. *Functions of Matrices: Theory and Computation*. Society for Industrial and Applied Mathematics, Philadelphia, PA, USA, 2008.
- [41] Yuji Nakatsukasa and Roland W. Freund. Computing Fundamental Matrix Decompositions Accurately via the Matrix Sign Function in Two Iterations: The Power of Zolotarev’s Functions. *SIAM Review*, 58(3):461–493, 2016.
- [42] Ming Gu and Stanley C. Eisenstat. Efficient algorithms for computing a strong rank-revealing QR factorization. 17(4):848–869, 1996.
- [43] Per-Gunnar Martinsson. Blocked rank-revealing QR factorizations: How randomized sampling can be used to avoid single-vector pivoting. *arXiv preprint arXiv:1505.08115*, 2015.
- [44] Grey Ballard, James Demmel, and Ioana Dumitriu. Minimizing Communication for Eigenproblems and the Singular Value Decomposition. *CoRR*, abs/1011.3077, 2010.
- [45] Hatem Ltaief, Dalal Sukkari, Aniello Esposito, Yuji Nakatsukasa, and David Keyes. Massively Parallel Polar Decomposition on Distributed-Memory Systems. *ACM Trans. Parallel Comput.*, 6(1), June 2019.